Advanced Composite Materials
Publication details, including instructions for authors and subscription information:
http://www.tandfonline.com/loi/tacm20

Effect of strain rate on nonlinear deformation behavior in CFRP composites

Keiji Ogi [a] & Nobuo Takeda [b]

[a] Research Institute for Applied Mechanics, Kyushu University, 6-1 Kasuga-Koen, Kasuga-city, Fukuoka 816, Japan

[b] Research Center for Advanced Science and Technology, The University of Tokyo, 4-6-1 Komaba, Meguro-ku, Tokyo 153, Japan

Version of record first published: 02 Apr 2012.

To cite this article: Keiji Ogi & Nobuo Takeda (1997): Effect of strain rate on nonlinear deformation behavior in CFRP composites, Advanced Composite Materials, 6:3, 175-196

To link to this article: http://dx.doi.org/10.1163/156855197X00067

Adv. Composite Mater., Vol. 6, No. 3, pp. 175–196 (1997)

Effect of strain rate on nonlinear deformation behavior in CFRP composites

KEIJI OGI[1,*] and NOBUO TAKEDA[2]

[1]*Research Institute for Applied Mechanics, Kyushu University, 6-1 Kasuga-Koen, Kasuga-city, Fukuoka 816, Japan*

[2]*Research Center for Advanced Science and Technology, The University of Tokyo, 4-6-1 Komaba, Meguro-ku, Tokyo 153, Japan*

Received 23 February 1996; accepted 3 June 1996

Abstract—This paper presents the effect of strain rates on nonlinear deformation behavior of CFRP composites. An elastic–plastic constitutive model is developed on the basis of both a complementary elastic energy function and a plastic potential, assuming that linear elastic deformation occurs in the fiber direction and that nonlinear strain in the shear direction is decomposed into nonlinear elastic strain and plastic strain. A one-parameter and a two-parameter plastic potential are employed to describe post-yielding behavior of composite laminae. Nonlinear elastic shear strain is measured by means of loading/unloading tensile tests of $[\pm 45^\circ]_S$ specimens. Off-axis tensile tests are performed to obtain the universal effective stress–effective plastic strain relation under monotonic loading. It is shown that rate-dependence of effective stress–effective plastic strain relation can be explained by determining anisotropy parameters of the plastic potential as functions of initial effective plastic strain rate.

Keywords: nonlinear deformation; CFRP; strain rate; plastic potential; off-axis test.

1. INTRODUCTION

Carbon fiber reinforced plastics (CFRPs) have been extensively employed in various engineering fields. Stress–strain response of CFRP laminates provides essential data in the application of CFRP laminates to light-weight structures, such as an aerospace vehicle.

Many theoretical models for inelastic behavior of CFRPs proposed in previous studies can be classified into three categories: nonlinear elasticity model, plasticity-based model and damage mechanics model. Hahn and Tsai [1] obtained a constitutive relation using a complementary elastic energy function. They introduced a fourth-order nonlinear term in the shear direction to describe nonlinear stress–strain behavior

*Author to whom correspondence should be sent.

of composite laminae. Jones and Morgan [2] developed a nonlinear constitutive model based on an elastic energy function. Hashin *et al.* [3] applied the Ramberg–Osgood relation to inelastic behavior of composites in the transverse and shear directions. The above models belong to nonlinear elasticity theories. On the other hand, plasticity-based theories have been studied by many researchers. Sun and Chen [4] proposed a one-parameter plasticity model using a quadratic plastic potential. Vaziri *et al.* [5] developed an orthotropic plasticity model including prediction of failure strength. Hansen *et al.* [6] presented an invariant flow rule for anisotropic plasticity using a scalar hardening parameter. Chaw and Yang [7] developed a damage mechanics model analogous to a flow rule employing a two-parameter damage potential.

Time-dependent behavior of inelastic response of the composites has been treated mainly by using viscoplasticity theories. Eisenberg and Yen [8] and Krempl and Hong [9] employed an overstress model to describe viscoplastic behavior of CFRP composites. Gates and Sun [10] applied a one-parameter plasticity model to the overstress concept.

In the present study, a two-dimensional macromechanical constitutive model is established on the basis of both nonlinear elasticity and plasticity theories using a complementary energy function and plastic potentials. Nonlinear strain in the longitudinal shear direction is assumed to be decomposed into nonlinear elastic strain and plastic strain. Two plastic constitutive equations are derived from a one-parameter and a two-parameter plastic potential. On-axis and off-axis tensile tests are conducted at various strain rates to determine elastic constants and plastic parameters regulating the effective stress–effective plastic strain relation. Off-axis tensile stress–strain responses predicted by the two plasticity models are compared with experimental results. The effect of strain rates on nonlinear stress–strain behavior is experimentally investigated and theoretically explained by expressing elastic constants and plastic parameters as functions of effective plastic strain rates.

2. THEORETICAL MODEL

2.1. Constitutive model

2.1.1. Nonlinear elasticity model. We consider an orthotropic lamina in a plane-stress state. On-axis and off-axis coordinate systems are defined in Fig. 1. Stresses in the fiber, transverse and longitudinal shear directions are denoted by σ_1, σ_2 and σ_6, respectively. It is assumed that (i) there is no nonlinearity in the fiber direction, (ii) there is no coupling between σ_1 and σ_6, and (iii) there is no nonlinear coupling between σ_1 and σ_2. Hence, a fourth-order complementary energy function W_C proposed by Hahn and Tsai [1] is rewritten as

$$W_C = \frac{1}{2}s_{11}\sigma_1^2 + \frac{1}{2}s_{22}\sigma_2^2 + \frac{1}{2}s_{66}\sigma_6^2 + s_{12}\sigma_1\sigma_2 + \frac{1}{3}s_{222}\sigma_2^3 + s_{266}\sigma_2\sigma_6^2 + \frac{1}{4}s_{2222}\sigma_2^4 + \frac{1}{4}s_{6666}\sigma_6^4 + s_{2266}\sigma_2^2\sigma_6^2, \tag{1}$$

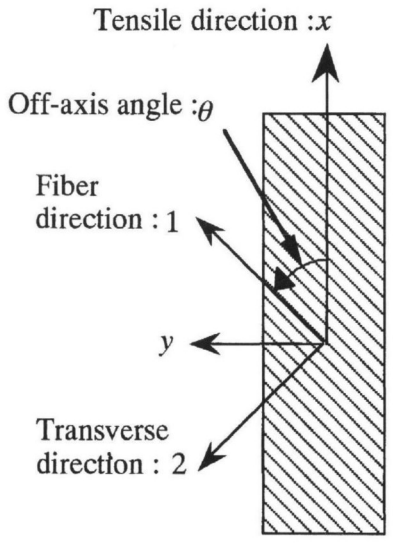

Figure 1. Definition of on-axis and off-axis coordinate systems denoted by (1, 2) and (x, y), respectively. The coordinate system (1, 2) coincides with material principal axes.

where s_{ij}, s_{ijk} and s_{ijkl} are the second-order, third-order and fourth-order coefficients. This function contains nonlinearity in both the transverse and longitudinal shear directions and shear coupling between the two directions. Differentiation of the complementary energy function with respect to each stress leads to the corresponding elastic strain:

$$\varepsilon_i^{\mathrm{e}} = \frac{\partial W_{\mathrm{C}}}{\partial \sigma_i}, \quad i = 1, 2, 6. \tag{2}$$

Thus, the elastic constitutive equation is obtained in the incremental form as follows:

$$\begin{Bmatrix} \mathrm{d}\varepsilon_1^{\mathrm{e}} \\ \mathrm{d}\varepsilon_2^{\mathrm{e}} \\ \mathrm{d}\varepsilon_6^{\mathrm{e}} \end{Bmatrix} = \begin{bmatrix} S_{11}^{\mathrm{e}} & S_{12}^{\mathrm{e}} & S_{16}^{\mathrm{e}} \\ & S_{22}^{\mathrm{e}} & S_{26}^{\mathrm{e}} \\ Sym. & & S_{66}^{\mathrm{e}} \end{bmatrix} \begin{Bmatrix} \mathrm{d}\sigma_1 \\ \mathrm{d}\sigma_2 \\ \mathrm{d}\sigma_6 \end{Bmatrix}, \tag{3}$$

where $\varepsilon_1^{\mathrm{e}}$, $\varepsilon_2^{\mathrm{e}}$ and $\varepsilon_6^{\mathrm{e}}$ are engineering elastic strains in the fiber, transverse and longitudinal shear directions, respectively, and S_{ij}^{e} are components of an elastic compliance matrix expressed as

$$\begin{aligned} &S_{11}^{\mathrm{e}} = s_{11}, \qquad S_{12}^{\mathrm{e}} = S_{21}^{\mathrm{e}} = s_{12}, \qquad S_{16}^{\mathrm{e}} = S_{61}^{\mathrm{e}} = 0, \\ &S_{22}^{\mathrm{e}} = s_{22} + 2s_{222}\sigma_2 + 3s_{2222}\sigma_2^2 + 2s_{2266}\sigma_6^2, \\ &S_{26}^{\mathrm{e}} = S_{62}^{\mathrm{e}} = 2s_{266}\sigma_6 + 4s_{2266}\sigma_2\sigma_6, \\ &S_{66}^{\mathrm{e}} = s_{66} + 2s_{266}\sigma_2 + 2s_{2266}\sigma_2^2 + 3s_{6666}\sigma_6^2. \end{aligned} \tag{4}$$

In our previous study [11], we confirmed from loading/unloading tests of [45°] and [90°] specimens that plastic deformation follows linear elastic deformation in

the transverse direction and that nonlinear elastic deformation does not occur in the transverse-shear coupling direction. In the shear direction, however, nonlinear elastic strain is observed in loading/unloading tensile test of $[\pm 45^\circ]_S$ specimens. Thus,

$$s_{222} = s_{2222} = s_{2266} = s_{266} = 0, \qquad s_{6666} \neq 0 \tag{5}$$

is derived. Substituting equation (5) into equation (4), we obtain

$$\begin{Bmatrix} d\varepsilon_1^e \\ d\varepsilon_2^e \\ d\varepsilon_6^e \end{Bmatrix} = \begin{bmatrix} s_{11} & s_{12} & 0 \\ & s_{22} & 0 \\ Sym. & & s_{66} + 3s_{6666}\sigma_6^2 \end{bmatrix} \begin{Bmatrix} d\sigma_1 \\ d\sigma_2 \\ d\sigma_6 \end{Bmatrix}. \tag{6}$$

As a result, this elastic constitutive equation has the same form as that derived by Hahn and Tsai [1]. In the present model, however, nonlinearity is assumed to be ascribed not only to nonlinear elastic deformation but also to plastic deformation. Nonlinear strain observed in the transverse direction and most part of nonlinear strain in the shear direction are proved to be due to plastic deformation [11]. Hence, in addition to the above elastic constitutive equation, plastic constitutive equations are established in the next section.

2.1.2. Plasticity model. Plastic strain increments are expressed using a plastic potential according to the associated flow rule as

$$d\varepsilon_i^p = \frac{\partial f}{\partial \sigma_i} d\lambda, \tag{7}$$

where $d\lambda$ is a proportional factor increment which is a function of stresses determined from the effective stress–effective plastic strain relation. Because nonlinear stress–strain behavior under monotonic loading is investigated in the present study, effects of a loading path on plastic deformation and Bauschinger effect are neglected. A yield criterion is expressed using the plastic potential as

$$f(\sigma_i) - k = 0, \tag{8}$$

where k stands for a measure of hardening which increases with effective plastic strain. The following quadratic plastic potential is employed:

$$f(\sigma_i) = \frac{1}{2} A_{ij}(k)\sigma_i\sigma_j, \tag{9}$$

where coefficients $A_{ij}(k)$ are anisotropy parameters. It should be noted that the summation convention is applied to equation (9). For strongly orthotropic fiber composites, it is not reasonable to assume that anisotropy parameters are constant [5]. Hence, we assume that the anisotropy parameters are functions of scalar k in the first step of the present model.

Effective stress and effective plastic strain are defined by

$$\sigma_e = \sqrt{3f}, \tag{10}$$

$$d\varepsilon_e^p = \frac{dW^p}{\sigma_e}, \tag{11}$$

where dW^p is plastic work increment defined by

$$dW^p = \sigma_i d\varepsilon_i^p. \tag{12}$$

From equations (7) to (12), we obtain

$$d\lambda = \frac{3}{2}\frac{d\varepsilon_e^p}{\sigma_e} = \frac{dk}{\frac{4}{9}\frac{d\sigma_e}{d\varepsilon_e^p}\sigma_e^2} = \frac{A_{ij}(k)\sigma_i d\sigma_j}{g\Omega}, \tag{13}$$

where

$$g = \frac{4}{9}\frac{d\sigma_e}{d\varepsilon_e^p}\sigma_e^2, \tag{14}$$

$$\Omega = 1 - \frac{1}{2}\sigma_i\sigma_j\frac{dA_{ij}(k)}{dk}. \tag{15}$$

The function g is determined from the effective stress–effective plastic strain relation, and the function Ω is obtained if A_{ij} are given as functions of k.

Substitution of equation (13) into equation (7) leads to

$$d\varepsilon_i^p = \frac{\partial f}{\partial \sigma_i}\frac{A_{pq}(k)\sigma_p d\sigma_q}{g\Omega}. \tag{16}$$

If all the anisotropy parameters are constant, the function Ω is unity and equation (16) is rewritten as

$$d\varepsilon_i^p = \frac{\partial f}{\partial \sigma_i}\frac{df}{g}. \tag{17}$$

The hardening model in which the anisotropy parameters change with plastic deformation has also been proposed by Vaziri *et al.* [5]. In their paper, however, expressions for the anisotropy parameters were not described clearly.

For fiber composites in the plane-stress state, the following two plastic potentials can be derived from an assumption of no plastic deformation in the fiber direction:

$$f = \frac{1}{2}\left(\sigma_2^2 + a_{66}(k)\sigma_6^2\right), \tag{18}$$

$$f = \frac{1}{2}\left(\sigma_2^2 + 2a_{26}(k)\sigma_2\sigma_6 + a_{66}(k)\sigma_6^2\right), \tag{19}$$

where a_{26} and a_{66} are used instead of A_{26}/A_{22} and A_{66}/A_{22}, respectively. A one-parameter plastic potential given by equation (18) has been proposed by Sun and Chen [4]; on the other hand, equation (19) is a two-parameter plastic potential which has been employed by Chaw and Yang [7] as a damage potential. They introduced a shear coupling effect in the damage potential assuming that matrix crack and/or matrix–fiber debonding have influence on deformation in both the transverse and shear directions. Here, we establish the following two plasticity models. In Model A, equation (18) is used as a plastic potential, in which the anisotropy parameter $a_{66}(k)$ is the following first order function of a scalar k:

$$a_{66}(k) = a_{66}{}^0 - \alpha\left[k - \frac{(\sigma_e{}^0)^2}{3}\right], \tag{20}$$

where α, $a_{66}{}^0$ and $\sigma_e{}^0$ are a rate of decrease in a_{66}, an initial value of a_{66}, and effective yield stress, respectively. On the other hand, in Model B, the two-parameter plastic potential expressed by equation (19) is employed although the two parameters are assumed to be constant:

$$a_{26}(k) = a_{26}{}^0, \qquad a_{66}(k) = a_{66}{}^0. \tag{21}$$

The effective stress–effective plastic strain relation is approximated by the following power law for Models A and B:

$$\sigma_e = B(\varepsilon_e^p)^m + \sigma_e{}^0, \tag{22}$$

where B and m are material constants which depend on temperature and strain rate. The exponent m means the inverse of the hardening parameter n. Sun and Chen's model [4], we set

$$\sigma_e{}^0 = 0, \qquad \frac{1}{m} = n, \qquad \frac{1}{B^{1/m}} = A. \tag{23}$$

Then, equation (22) yields

$$\varepsilon_e^p = A\sigma_e^n \tag{24}$$

for Sun and Chen's model. Vaziri *et al.* [5] assumed the bilinear hardening, which corresponds to $m = 1$ in equation (22). Using equations (18) to (22), equations (14) and (15) yield

$$g = \frac{4}{9} m B^{1/m} \sigma_e^2 (\sigma_e - \sigma_e{}^0)^{(1-m)/m}, \quad \text{for Models A and B,} \tag{25}$$

$$\begin{cases} \Omega = 1 + \dfrac{\alpha}{2}\sigma_6^2, & \text{for Model A,} \\ \Omega = 1, & \text{for Model B.} \end{cases} \tag{26}$$

In Sun and Chen's model, $\sigma_e{}^0 = 0$ and $\alpha = 0$ are used in Model A.

Finally, a plastic constitutive equation is presented for Models A and B from equations (16), (18) and (19) as

$$\begin{Bmatrix} d\varepsilon_1^p \\ d\varepsilon_2^p \\ d\varepsilon_6^p \end{Bmatrix} = \frac{1}{g\Omega} \begin{bmatrix} 0 & 0 & 0 \\ & \sigma_2^2 & a_{66}(k)\sigma_2\sigma_6 \\ Sym. & & \{a_{66}(k)\}^2\sigma_6^2 \end{bmatrix} \begin{Bmatrix} d\sigma_1 \\ d\sigma_2 \\ d\sigma_6 \end{Bmatrix}, \quad \text{for Model A,} \tag{27}$$

$$\begin{Bmatrix} d\varepsilon_1^p \\ d\varepsilon_2^p \\ d\varepsilon_6^p \end{Bmatrix} = \frac{1}{g} \begin{bmatrix} 0 & 0 & 0 \\ & (\sigma_2 + a_{26}\sigma_6)^2 & (\sigma_2 + a_{26}\sigma_6)(a_{26}\sigma_2 + a_{66}\sigma_6) \\ Sym. & & (a_{26}\sigma_2 + a_{66}\sigma_6)^2 \end{bmatrix} \begin{Bmatrix} d\sigma_1 \\ d\sigma_2 \\ d\sigma_6 \end{Bmatrix},$$

for Model B. (28)

Substitution of $a_{66}(k) = a_{66}{}^0$ and $\Omega = 1$ into equation (27) leads to the plastic constitutive equation for Sun and Chen's model.

2.1.3. Elastic–plastic constitutive equation. Total strain increment is decomposed into elastic strain increment and plastic strain increment expressed by

$$d\varepsilon_i = d\varepsilon_i^e + d\varepsilon_i^p \tag{29}$$

or

$$\begin{Bmatrix} d\varepsilon_1 \\ d\varepsilon_2 \\ d\varepsilon_6 \end{Bmatrix} = \begin{bmatrix} S_{11} & S_{12} & S_{16} \\ & S_{22} & S_{26} \\ Sym. & & S_{66} \end{bmatrix} \begin{Bmatrix} d\sigma_1 \\ d\sigma_2 \\ d\sigma_6 \end{Bmatrix}, \tag{30}$$

where S_{ij} are components of an elastic–plastic compliance matrix. From equations (6) and (27), these components are given by

$$\begin{aligned} &S_{11} = s_{11}, \qquad S_{12} = S_{21} = s_{12}, \qquad S_{16} = S_{61} = 0, \\ &S_{22} = s_{22} + \frac{\sigma_2^2}{g\Omega}, \\ &S_{26} = S_{62} = \frac{a_{66}(k)\sigma_2\sigma_6}{g\Omega}, \\ &S_{66} = s_{66} + 3s_{6666}\sigma_6^2 + \frac{\{a_{66}(k)\}^2\sigma_6^2}{g\Omega}, \quad \text{for Model A.} \end{aligned} \tag{31}$$

From equations (6) and (28), we can obtain

$$
\begin{aligned}
&S_{11} = s_{11}, \qquad S_{12} = S_{21} = s_{12}, \qquad S_{16} = S_{61} = 0, \\
&S_{22} = s_{22} + \frac{(\sigma_2 + a_{26}\sigma_6)^2}{g}, \\
&S_{26} = S_{62} = \frac{(\sigma_2 + a_{26}\sigma_6)(a_{26}\sigma_2 + a_{66}\sigma_6)}{g}, \\
&S_{66} = s_{66} + 3s_{6666}\sigma_6^2 + \frac{(a_{26}\sigma_2 + a_{66}\sigma_6)^2}{g}, \quad \text{for Model B.}
\end{aligned}
\tag{32}
$$

2.2. *Off-axis tensile tests*

2.2.1. Effective stress–effective plastic strain relation. The effective stress–effective plastic strain relation is determined by off-axis monotonic tensile tests. The stresses referring to the material principal axes, or the on-axis coordinate system in Fig. 1, are expressed using the off-axis tensile stress σ_x as

$$
\sigma_1 = \cos^2\theta\sigma_x, \qquad \sigma_2 = \sin^2\theta\sigma_x, \qquad \sigma_6 = -\sin\theta\cos\theta\sigma_x, \tag{33}
$$

where θ is an off-axis angle defined in Fig. 1. From equations (8), (10), (18), (20) and (33), the effective stress for Model A is expressed as

$$
\sigma_e = \frac{F(\theta)\sigma_x}{\sqrt{1 + G(\theta)\sigma_x^2}}, \tag{34}
$$

where $F(\theta)$ and $G(\theta)$ are the following functions of the off-axis angle:

$$
F(\theta) = \sqrt{\frac{3}{2}\sin^4\theta + \frac{1}{2}\left\{3a_{66}{}^0 + \alpha\left(\sigma_e{}^0\right)^2\right\}\sin^2\theta\cos^2\theta}, \tag{35}
$$

$$
G(\theta) = \frac{1}{2}\alpha\sin^2\theta\cos^2\theta. \tag{36}
$$

From equations (10), (19), (21) and (33), we obtain the effective stress for Model B as

$$
\sigma_e = H(\theta)\sigma_x, \tag{37}
$$

where

$$
H(\theta) = \sqrt{\frac{3}{2}\left(\sin^4\theta - 2a_{26}{}^0\sin^3\theta\cos\theta + a_{66}{}^0\sin^2\theta\cos^2\theta\right)}. \tag{38}
$$

Plastic strain increment in the off-axis tensile direction is expressed as

$$
\mathrm{d}\varepsilon_x^p = \cos^2\theta\mathrm{d}\varepsilon_1^p + \sin^2\theta\mathrm{d}\varepsilon_2^p - \sin\theta\cos\theta\mathrm{d}\varepsilon_6^p. \tag{39}
$$

For Model A, plastic strain increments in the material principal directions are calculated from equations (7) and (18) as

$$d\varepsilon_1^p = 0, \qquad d\varepsilon_2^p = \sigma_2 d\lambda, \qquad d\varepsilon_6^p = a_{66}(k)\sigma_6 d\lambda. \tag{40}$$

Substitution of equation (40) into equation (39) using equations (20), (33) and (34) leads to

$$d\varepsilon_x^p = \frac{2}{3}\frac{\{F(\theta)\}^2\sigma_x}{1+G(\theta)\sigma_x^2}d\lambda. \tag{41}$$

From equations (13), (34) and (41), we can derive the effective plastic strain increment for Model A using the off-axis tensile plastic strain increment:

$$d\varepsilon_e^p = \frac{\sqrt{1+G(\theta)\sigma_x^2}}{F(\theta)}d\varepsilon_x^p. \tag{42}$$

Similarly, the effective plastic strain increment for Model B is obtained as

$$d\varepsilon_e^p = \frac{d\varepsilon_x^p}{H(\theta)}. \tag{43}$$

By integrating equations (42) and (43), we obtain the effective plastic strain as

$$\varepsilon_e^p = \int \frac{\sqrt{1+G(\theta)\sigma_x^2}}{F(\theta)}d\varepsilon_x^p, \quad \text{for Model A,} \tag{44}$$

$$\varepsilon_e^p = \frac{\varepsilon_x^p}{H(\theta)}, \quad \text{for Model B.} \tag{45}$$

In Sun and Chen's model [4], $\alpha = 0$ is substituted into equations (34) and (44) since a one-parameter plastic potential in which the anisotropy parameter is constant is employed in their model. Hence, the effective stress and effective plastic strain for Sun and Chen's model expressed as

$$\sigma_e = F_0(\theta)\sigma_x, \tag{46}$$

$$\varepsilon_e^p = \frac{\varepsilon_x^p}{F_0(\theta)}, \tag{47}$$

where

$$F_0(\theta) = F(\theta)\big|_{\alpha=0} = \sqrt{\frac{3}{2}\left(\sin^4\theta + a_{66}{}^0\sin^2\theta\cos^2\theta\right)}. \tag{48}$$

Here, we assume that the universal effective stress–effective plastic strain relation is obtained when the composite is loaded in tension at the same initial effective plastic strain rate under various combined stress conditions. The initial effective

plastic strain rate is defined as the effective plastic strain rate at the onset of plastic deformation:

$$\left(\dot{\varepsilon}_e^p\right)^0 = \left.\frac{d\varepsilon_e^p}{dt}\right|_{\varepsilon_e^p=0}. \tag{49}$$

For Models A and B, the initial effective plastic strain rates are expressed from equations (44) and (45), respectively, as

$$\left(\dot{\varepsilon}_e^p\right)^0 = \frac{\dot{\varepsilon}_x^p}{F_0(\theta)}, \quad \text{for Model A,} \tag{49}$$

$$\left(\dot{\varepsilon}_e^p\right)^0 = \frac{\dot{\varepsilon}_x^p}{H(\theta)}, \quad \text{for Model B.} \tag{50}$$

The plastic parameters are determined as follows. First, for Models A and B, the effective yield stress defined as the stress at the beginning of plastic deformation is calculated using equations (34) and (37) as

$$\sigma_e{}^0 = F_0(45^\circ)R, \qquad \sigma_e{}^0 = F_0(90^\circ)Y, \tag{51}$$

where Y and R are the yield stresses of a [90°] and a [45°] specimen, respectively. By eliminating $\sigma_e{}^0$ from equation (51), we obtain an initial value of the anisotropy parameter a_{66} for Model A:

$$a_{66}{}^0 = 2\left(\frac{Y}{R}\right)^2 - \frac{1}{2}. \tag{52}$$

Next, if an appropriate value of α is given, the functions $F(\theta)$ and $G(\theta)$ expressed by equations (35) and (36), respectively, are calculated for each off-axis angle. Then, the effective stress and the effective plastic strain are computed using equations (34) and (44) from a tensile stress–plastic strain curve of each off-axis specimen. The value of α is determined so that the effective stress–effective plastic strain plots for various off-axis angles are reduced to one master curve. By curve-fitting of the universal effective stress–effective plastic strain curve using equation (22), a coefficient B and an exponent m are determined.

On the other hand, in Model B, longitudinal and transverse plastic strain increments are expressed as

$$\begin{aligned} d\varepsilon_x^p &= \cos^2\theta\, d\varepsilon_1^p + \sin^2\theta\, d\varepsilon_2^p - \sin\theta\cos\theta\, d\varepsilon_6^p, \\ d\varepsilon_y^p &= \sin^2\theta\, d\varepsilon_1^p + \cos^2\theta\, d\varepsilon_2^p + \sin\theta\cos\theta\, d\varepsilon_6^p. \end{aligned} \tag{53}$$

Using equations (7), (19), (21) and (33), equation (53) is rewritten as

$$\begin{aligned} d\varepsilon_x^p &= \left(\sin^4\theta - 2a_{26}{}^0\sin^3\theta\cos\theta + a_{66}{}^0\sin^2\theta\cos^2\theta\right)\sigma_x d\lambda, \\ d\varepsilon_y^p &= \left\{a_{26}{}^0(\sin^3\theta\cos\theta - \sin\theta\cos^3\theta) + (1 - a_{66}{}^0)\sin^2\theta\cos^2\theta\right\}\sigma_x d\lambda. \end{aligned} \tag{54}$$

Then, plastic Poisson's ratio is expressed for Model B as

$$v_{xy}^{\mathrm{p}} = -\frac{\mathrm{d}\varepsilon_y^{\mathrm{p}}}{\mathrm{d}\varepsilon_x^{\mathrm{p}}} = \frac{a_{26}{}^0\left(1-\tan^2\theta\right)+\left(a_{66}{}^0-1\right)\tan\theta}{\tan^3\theta-2a_{26}{}^0\tan^2\theta+a_{66}{}^0\tan\theta}. \tag{55}$$

When plastic Poisson's ratio measured for two different off-axis angles, the two anisotropy parameters $a_{26}{}^0$ and $a_{66}{}^0$ are computed using equation (55). The effective stress–effective plastic strain plots obtained from equations (37) and (45) for various off-axis angles are fitted by equation (22) to determine a coefficient B and an exponent m.

2.2.2. Off-axis tensile stress–strain response. Total stress–strain response of an off-axis specimen is predicted using the elastic constants and the plastic parameters. First, tensile plastic strains for Models A and B are expressed as a function of tensile stress using equations (22), (34), (37), (42) and (43) as

$$\varepsilon_x^{\mathrm{p}} = \frac{\left\{F(\theta)\right\}^2}{mB}\int_{\sigma_x{}^0}^{\sigma_x}\frac{\left[\frac{1}{B}\left(\frac{F(\theta)\sigma_x}{\sqrt{1+G(\theta)\sigma_x^2}}-\sigma_{\mathrm{e}}{}^0\right)\right]^{(1-m)/m}}{\left(1+G(\theta)\sigma_x^2\right)^{5/2}}\,\mathrm{d}\sigma_x, \tag{56}$$

for Model A,

$$\varepsilon_x^{\mathrm{p}} = H(\theta)\left(\frac{H(\theta)\sigma_x-\sigma_{\mathrm{e}}{}^0}{B}\right)^{1/m}, \quad \text{for Model B,} \tag{57}$$

where $\sigma_x{}^0$ is tensile yield stress of an off-axis specimen. In Sun and Chen's model, tensile plastic strain is presented from equations (24), (46) and (47) as

$$\varepsilon_x^{\mathrm{p}} = AF_0(\theta)^{n+1}\sigma_x^n. \tag{58}$$

On the other hand, tensile elastic strain of an off-axis specimen is described as

$$\varepsilon_x^{\mathrm{e}} = \int\left[(\cos^4\theta)S_{11}^{\mathrm{e}}+(\sin^4\theta)S_{22}^{\mathrm{e}}+(2\sin^2\theta\cos^2\theta)S_{12}^{\mathrm{e}}+(\sin^2\theta\cos^2\theta)S_{66}^{\mathrm{e}}\right]\mathrm{d}\sigma_x. \tag{59}$$

Using the components of the elastic compliance in equation (6), equation (59) yields

$$\varepsilon_x^{\mathrm{e}} = s_{xx}\sigma_x + s_{xxxx}\sigma_x^3, \tag{60}$$

where

$$\begin{aligned} s_{xx} &= (\cos^4\theta)s_{11}+(\sin^4\theta)s_{22}+(2\sin^2\theta\cos^2\theta)s_{12}+(\sin^2\theta\cos^2\theta)s_{66},\\ s_{xxxx} &= (\sin^4\theta\cos^4\theta)s_{6666}. \end{aligned} \tag{61}$$

Finally, total tensile strain decomposed into tensile elastic strain and tensile plastic strain is given as a function of tensile strain using equation (60) as

$$\varepsilon_x = s_{xx}\sigma_x + s_{xxxx}\sigma_x^3 + \varepsilon_x^p. \tag{62}$$

The plastic strains for Models A and B and Sun and Chen's model are described in equations (56), (57) and (58), respectively. Actually, the nonlinear elastic strain is so small in comparison with plastic strain that it is possible to neglect the second term in equation (62).

3. EXPERIMENT

3.1. Material

The material used was a graphite-fiber reinforced epoxy matrix composite (T300/#2500, Toray). The composite plates were cured at a temperature of 120°C and the final fiber volume fraction was 0.58. The coupon specimens were cut from unidirectional plates (300 × 500 × 2.8 mm^3) and [±45°] symmetric laminates (300 × 300 × 0.6 mm^3). The specimens have lengths of 150–200 mm and widths of 10–20 mm. The on-axis and off-axis specimens ([0°], [30°], [45°], [60°], [90°]) were cut from the unidirectional plates. Tapered aluminum tabs were bonded on both ends of the specimen using an epoxy adhesive for high temperature testing up to 250°C. The specimens were dried in a vacuum chamber at 30°C for one month before tensile tests.

3.2. Experimental procedure

Monotonic and loading/unloading tensile tests were conducted using the data acquisition system for load-strain measurement as illustrated in Fig. 2. An electro-hydraulic

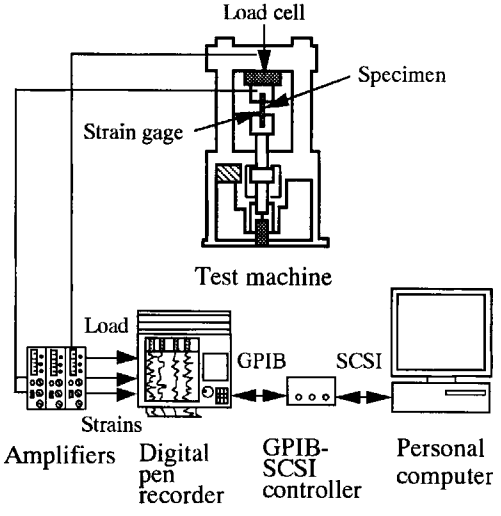

Figure 2. Data acquisition system for stress–strain measurement.

fatigue test machine was used for tensile tests. A specimen was kept at a constant temperature of 70°C for 60 min in a thermostatic chamber to ensure the temperature uniformity of the specimen. The strains in two or three different directions were measured with rosette (0°/90° or 0°/45°/90°) strain gages mounted on the specimen surface. The signals of the strain gages were amplified and input to a digital pen-recorder with the load signal. All the analog signals were converted to the digital ones in the pen-recorder and transferred to a personal computer. Monotonic tensile tests were conducted for on-axis and off-axis specimens at a temperature of 70°C at various strain rates. The strain rates of off-axis specimens were selected so that the initial effective plastic strain rate is almost the same among various off-axis specimens. Loading/unloading tensile tests were conducted for $[\pm 45°]_S$ specimens to measure nonlinear elastic strain in the shear direction. Since the permanent strain on unloading is defined as plastic strain, the nonlinear elastic strain was calculated by subtracting the plastic strain from the total nonlinear strain.

4. RESULTS AND DISCUSSION

Both longitudinal and transverse strains against longitudinal stress obtained from [0°] specimens are linear. These results confirm that the coefficients s_{11} and s_{12} are constant because of an observed linearity of the fiber stress–strain curve. Figure 3 shows transverse tensile stress–strain curves obtained from the tensile tests of [90°] specimens at three different strain rates. Slight nonlinearity is observed after yielding at which the curve shows a knee point. This nonlinearity is attributed not to nonlinear elasticity but to plastic deformation because permanent strain with the same value as

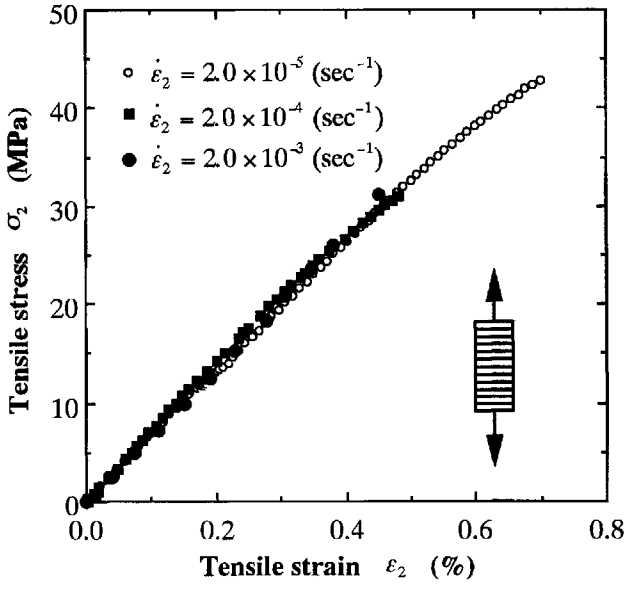

Figure 3. Tensile stress–strain curves of [90°] CF/Epoxy specimens for various strain rates at 70°C.

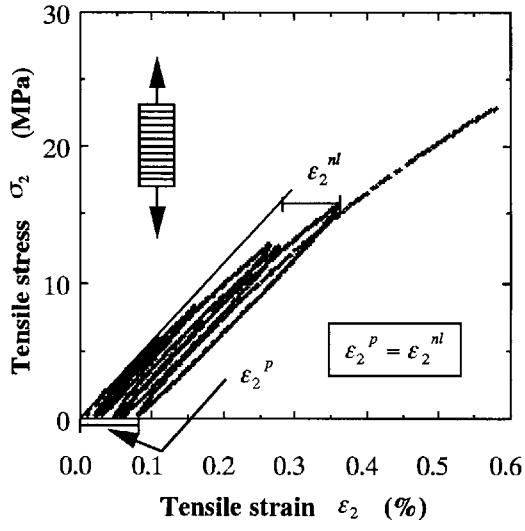

Figure 4. A loading/unloading stress–strain curve of a [90°] CF/Epoxy specimen at 70°C. Plastic strain with the same value as nonlinear strain is observed after full unloading.

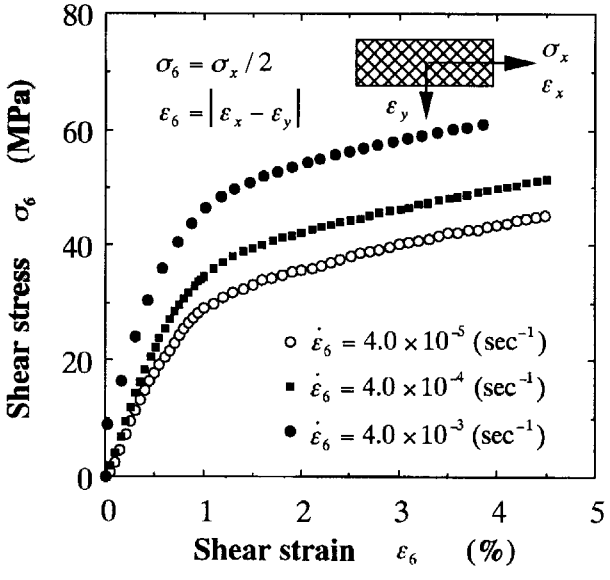

Figure 5. Effect of strain rate on shear stress–strain response obtained using $[\pm 45^\circ]_S$ CF/Epoxy specimens at 70°C.

nonlinear strain before unloading is observed after unloading. Figure 4 displays a loading/unloading stress–strain curve of a [90°] specimen at 70°C. Permanent (plastic) strain is observed on unloading, which is almost the same as the nonlinear strain on loading. Figure 5 shows the effect of strain rate on shear stress–strain response obtained using $[\pm 45^\circ]_S$ specimens. Remarkable rate-dependence is observed in initial shear modulus and post-yielding behavior. Figure 6 depicts shear stress–shear strain

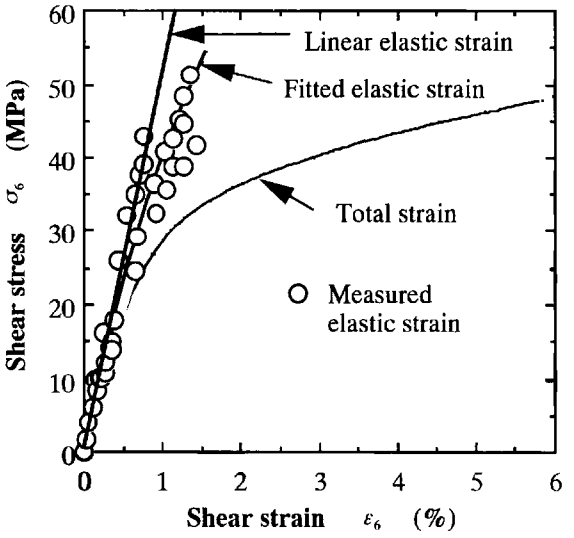

Figure 6. Shear stress–shear strain curve obtained by loading/unloading tests of five $[\pm 45^\circ]_S$ CF/Epoxy specimens at 70°C.

Table 1.
Rate-dependence of the elastic constants of CF/Epoxy composites at the temperature of 70°C

$(\dot{\varepsilon}_e^p)^0$ (s^{-1})	$s_{11} \times 10^3$ (GPa^{-1})	$s_{22} \times 10^1$ (GPa^{-1})	$s_{12} \times 10^3$ (GPa^{-1})	$s_{66} \times 10^1$ (GPa^{-1})	$s_{6666} \times 10^8$ (GPa^{-1})
2.0×10^{-3}	8.47	1.20	−2.54	1.92	-
2.0×10^{-4}	7.93	1.39	−2.62	2.08	2.75
2.0×10^{-5}	7.63	1.49	−2.51	2.27	-

plots obtained from loading/unloading tests of five $[\pm 45^\circ]_S$ specimens. The coefficients s_{66} and s_{6666} are determined by curve-fitting of the shear stress–elastic shear strain plots. Nonlinear elastic deformation ascribed to the fourth-order coefficient s_{6666} can be observed at high stresses. However, it is proved that nonlinearity in the shear direction is due chiefly to plastic deformation by the present tests. It should be noted that effects of damage (fiber/matrix interfacial debonding, delamination, matrix cracking) must be dominant in large deformation in measuring the shear properties using $[\pm 45^\circ]_S$ specimens. The elastic constants obtained for various strain rates are summarized in Table 1. Although elastic modulus in the fiber direction is insensitive to strain rates, the moduli in the transverse and shear directions show significant rate dependence.

In Fig. 7, the yield stresses of [90°] and [45°] specimens are plotted against the initial effective plastic strain rate. From this figure, yield stresses Y, R and the anisotropy parameter $a_{66}{}^0$ in Model A are expressed as functions of the initial effective plastic strain rate using the power law and equation (52):

$$Y = 53.7\left[\left(\dot{\varepsilon}_e^p\right)^0\right]^{0.0969}, \qquad R = 35.5\left[\left(\dot{\varepsilon}_e^p\right)^0\right]^{0.0376},$$
$$a_{66}{}^0 = 4.07\left[\left(\dot{\varepsilon}_e^p\right)^0\right]^{0.119} - 0.5. \tag{63}$$

The measured plastic Poisson's ratios for two off-axis angles 30° and 60° and the two anisotropy parameters $a_{26}{}^0$ and $a_{66}{}^0$ in Model B calculated using equation (55) are presented in Table 2 for three different initial plastic strain rates. The parameter $a_{26}{}^0$ has a negative value at a high plastic strain rate and increases with decreasing the plastic strain rate.

Effective stress–effective plastic strain curves at two initial effective plastic strain rates obtained using Model A, Model B and Sun and Chen's model are presented

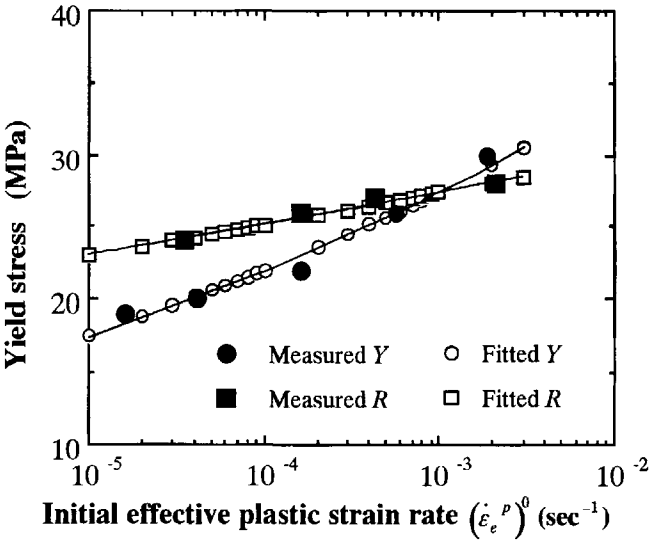

Figure 7. Measured yield stresses of [90°] and [45°] CF/Epoxy specimens plotted against the initial effective plastic strain rate.

Table 2.
Measured plastic Poisson's ratios and calculated anisotropy parameters of CF/Epoxy composites in Model B against the initial effective plastic strain rate

$(\dot{\varepsilon}_e^p)^0$ (s^{-1})	θ	ν_{xy}^p	$a_{66}{}^0$	$a_{26}{}^0$
2.0×10^{-3}	30°	0.641	**8.28**	−0.926
	60°	0.576		
2.0×10^{-4}	30°	0.810	**5.18**	0.137
	60°	0.522		
2.0×10^{-5}	30°	0.927	**5.38**	0.412
	60°	0.562		

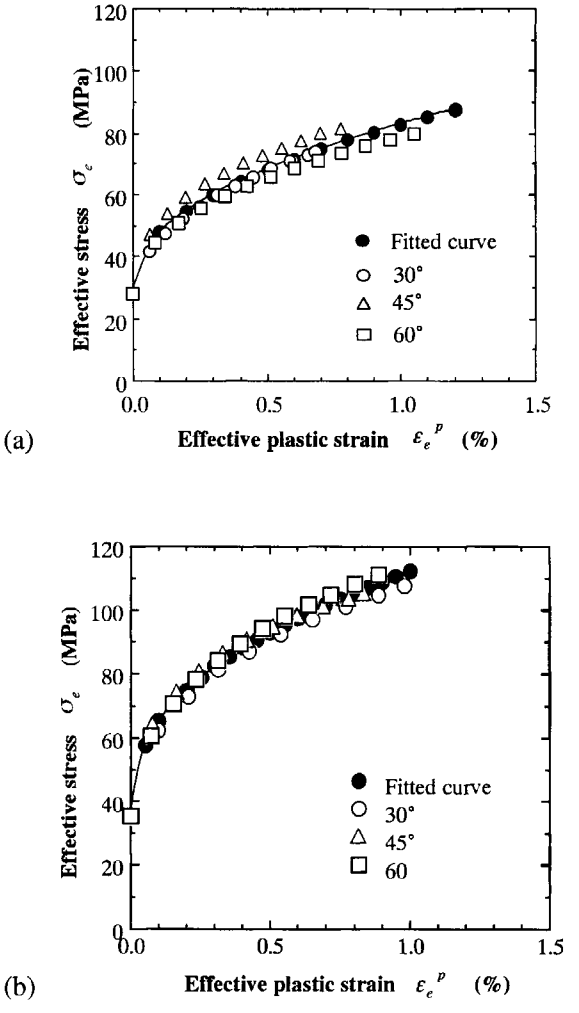

Figure 8. Effective stress–effective plastic strain curves obtained using Model A at the temperature of 70°C and the initial effective plastic strain rate of (a) 2×10^{-4} s^{-1}, (b) 2×10^{-3} s^{-1}.

in Figs 8, 9 and 10, respectively. The solid lines in those figures are obtained by curve–fitting using equation (22) for Models A and B, and using equation (24) for Sun and Chen's model. Effective stress in Models A and B and effective plastic strain in Model A are estimated to be larger than those obtained by Sun and Chen's model, but effective plastic strain computed by Model B is smaller than that calculated by Sun and Chen's model. The large effective stress and effective plastic strain in Model A are correlated with a decrease in the anisotropy parameter $a_{66}(k)$ with the plastic deformation. On the other hand, the large effective stress and the small effective plastic strain result from a larger value of function $H(\theta)$ than that of function $F_0(\theta)$. Effect of the initial effective plastic strain rate on the effective stress–effective plastic strain relation obtained by Model A is described in Fig. 11. Two curves are presented

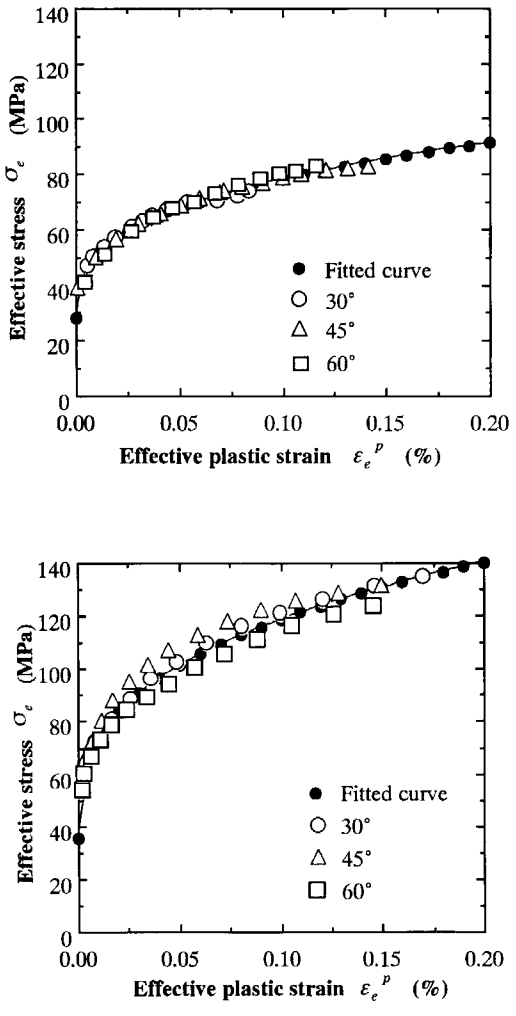

Figure 9. Effective stress–effective plastic strain curves obtained using Model B at the temperature of 70°C and the initial effective plastic strain rate of (a) 2×10^{-4} s^{-1}, (b) 2×10^{-3} s^{-1}.

for each strain rate; one is a curve for $\alpha > 0$ and the other is a curve for $\alpha = 0$, which is located above the curve for $\alpha > 0$. For $\alpha > 0$, the slope of the effective stress–effective plastic strain curve decreases as the anisotropic parameter $a_{66}(k)$ decreases with increasing scalar k (equation (20)), but $a_{66}(k)$ is constant for $\alpha = 0$. The plastic parameters in Models A and B and Sun and Chen's model obtained in Figs 8, 9 and 10, respectively, are presented for two initial effective plastic strain rates in Tables 3, 4, and 5, respectively. In Model A, while the initial value of the anisotropy parameter a_{66}, or $a_{66}{}^0$, depends on the initial effective plastic strain rate, the rate of decrease in a_{66}, or α, and the hardening parameter m are independent of strain rate (Table 3). Similar characteristics of rate dependence are shown in Model B (Table 4) and Sun and Chen's model (Table 5), namely, strain rate has remarkable effect on the anisotropy

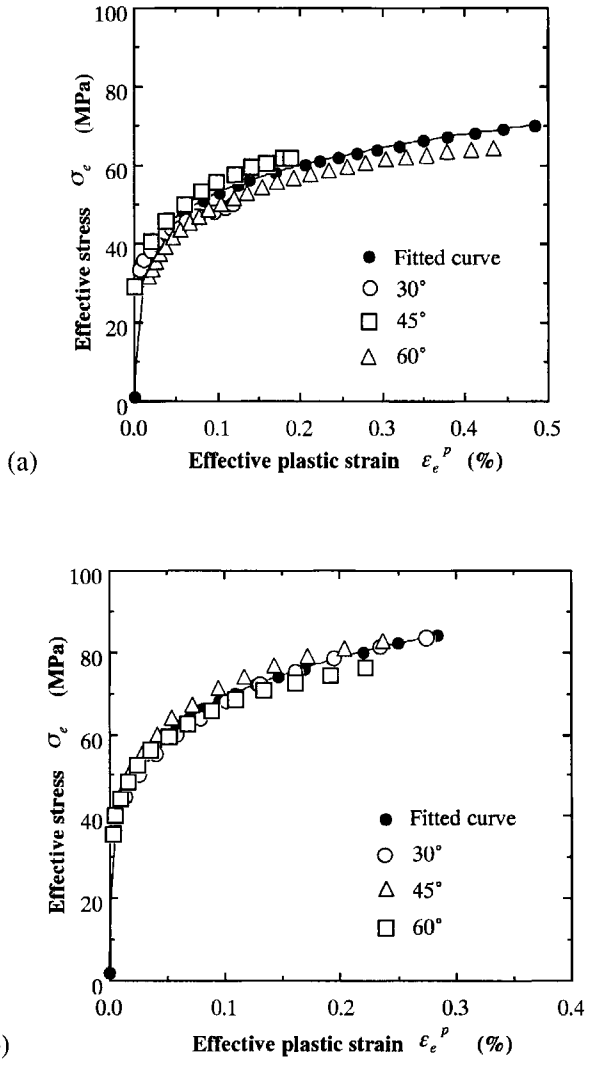

Figure 10. Effective stress–effective plastic strain curves obtained using Sun and Chen's model at the temperature of 70°C and the initial effective plastic strain rate of (a) 2×10^{-4} s^{-1}, (b) 2×10^{-3} s^{-1}.

parameters and relatively small influence on the hardening parameter m or n. These results contrast the effect of temperature on the plastic parameters in our previous study [11]. Notable temperature variation was observed in the parameters α and m or n, although effect of temperature on $a_{66}{}^0$ was rather small.

Figure 12 presents off-axis tensile stress–strain curves predicted by Models A and B and Sun and Chen's model compared with experimental results. The curve predicted by Model A shows the best agreement with experimental results among the curves predicted by the three models. Model A and Sun and Chen's model have one fitting parameter, which is α and $a_{66}{}^0$, respectively, but no fitting parameter is employed

Table 3.
The parameters concerned with plastic deformation employed in Model A

$(\dot{\varepsilon}_e^p)^0$ (s^{-1})	$a_{66}{}^0$	$\sigma_e{}^0$ (MPa)	α (MPa^{-2})	B (MPa)	m
2.0×10^{-4}	2.32	28.2	0.0000	66.73	0.49219
			0.0004	54.78	0.44882
2.0×10^{-3}	3.38	**35.5**	0.0000	103.7	0.50674
			0.0004	76.86	0.41527

Table 4.
The parameters concerned with plastic deformation employed in Model B

$(\dot{\varepsilon}_e^p)^0$ (s^{-1})	$\sigma_e{}^0$ (MPa)	B (MPa)	m
2.0×10^{-4}	28.2	109.2	0.3389
2.0×10^{-3}	35.5	179.2	0.3333

Table 5.
The parameters concerned with plastic deformation employed in Sun and Chen's model

$(\dot{\varepsilon}_e^p)^0$ (s^{-1})	a_{66}	A (MPa^{-n})	n
2.0×10^{-4}	2.32	2.612×10^{-13}	5.565
2.0×10^{-3}	3.38	2.506×10^{-13}	5.225

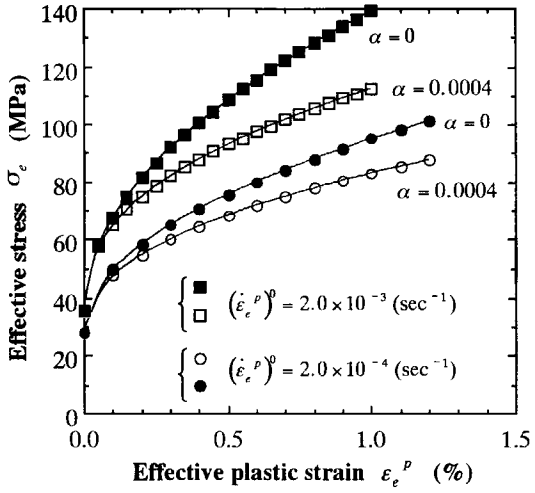

Figure 11. Effect of strain rate on effective stress–effective plastic strain curves at 70°C obtained using Model A. All curves are obtained by curve-fitting of the measured data of off-axis tensile tests.

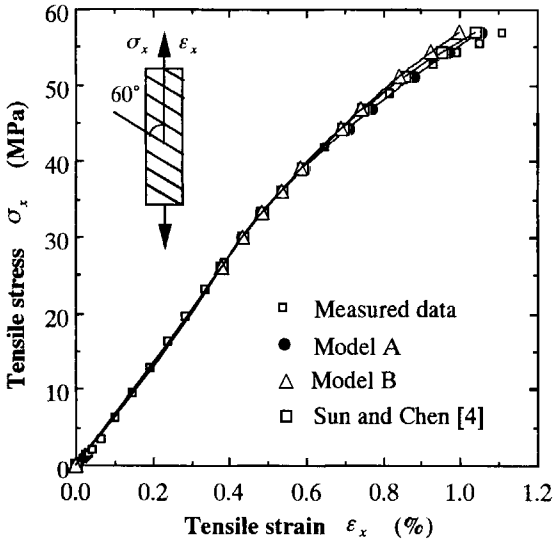

Figure 12. Comparison of off-axis tensile stress–strain curves predicted by the three models with experimental results. The off-axis angle, initial effective plastic strain rate and temperature are 60°, 2×10^{-3} s^{-1} and 70°C, respectively.

in Model B because the two anisotropy parameters ${a_{26}}^0$ and ${a_{66}}^0$ are empirically determined by measurement of plastic Poisson's ratio (equation (55)). Hence, off-axis stress–strain curves are not successfully predicted by Model B unless the two anisotropy parameters are accurately estimated.

5. CONCLUSIONS

The effect of strain rates on nonlinear deformation behavior in CFRP composites was investigated on the basis of a nonlinear elasticity theory and a flow rule. Two constitutive equations were formulated using a one-parameter and a two-parameter plastic potential. The elastic constants and the plastic parameters were determined by on-axis and off-axis tensile tests at various strain rates. Both nonlinear elastic deformation and plastic deformation were observed in the shear direction. Rate-dependence of the plastic parameters was examined using the initial effective plastic strain rate. Off-axis tensile stress–strain curves predicted by three plasticity models were compared with experimental results. Prediction by Model A that employs a one-parameter plastic potential in which the anisotropy parameter changes was the most successful.

REFERENCES

1. Hanh, H. T. and Tsai, S. W. Nonlinear elastic behavior of unidirectional composite laminae. *J. Compos. Mater.* **7**, 102–118 (1973).
2. Jones, R. M. and Morgan, H. S. Analysis of nonlinear stress–strain behavior of fiber-reinforced composite materials. *AIAA Journal* **15**, 1669–1676 (1977).

3. Hashin, Z., Bagchi, D. and Rosen, B. W. Nonlinear behavior of fiber coomposite laminates. *NASA CR* 2313 (1974).
4. Sun, C. T. and Chen, J. L. A simple flow rule for characterizing nonlinear behavior of fiber composites. *J. Compos. Mater.* **23**, 1009–1020 (1989).
5. Vaziri, R., Olson, M. S. and Anderson, D. L. A plastic-based constitutive model for fiber-reinforced composite laminates. *J. Compos. Mater.* **25**, 512–535 (1991).
6. Hansen, A. C., Blackketter, D. M. and Walrath, D. E An invariant-based flow rule for anisotropic plasticity applied to composite materials. *Trans. ASME, Ser. E, J. Appl. Mech.* **58**, 881–888 (1991).
7. Chaw, C. L. and Yang, F. A simple model for brittle composite lamina with damage. *J. Reinforced Plast. Compos.* **11**, 222–242 (1992).
8. Eisenberg, M. A. and Yen, C.-F. A theory of multiaxial anisotropic viscoplasticity. *Trans. ASME, Ser. E, J. Appl. Mech.* **48**, 276–284 (1981).
9. Krempl, E. and Hong, B. Z. A simple laminate theory using the orthotropic viscoplasticity theory based on overstress. Part I: In-plane stress–strain relationships for metal matrix composites. *Compos. Sci. Technol.* **35**, 53–74 (1989).
10. Gates, T. S. and Sun, C. T. Elastic/viscoplastic constitutive model for fiber reinforced thermoplastic composites. *AIAA Journal* **29**, 457–463 (1991).
11. Ogi, K. and Takeda, N. Effect of temperature on nonlinear tensile stress–strain behavior of CF/Epoxy composites. *J. Soc. Mater. Sci. Jpn.* **45**, 478–483 (1996) (in Japanese).